

Nanomechanical vibrational response from electrical mixing measurements

C. Samanta,¹ D. A. Czaplewski,² S. L. De Bonis,¹ C. B. Møller,¹ R. Tormo Queralt,¹ C. S. Miller,² Y. Jin,³ F. Pistolesi,⁴ and A. Bachtold¹

¹*ICFO - Institut De Ciències Fotoniques, The Barcelona Institute of Science and Technology, 08860 Castelldefels (Barcelona), Spain*

²*Center for Nanoscale Materials, Argonne National Laboratory, Argonne, IL, 60439, USA*

³*C2N, CNRS, Université Paris-Saclay, Palaiseau, France*

⁴*Université de Bordeaux, CNRS, LOMA, UMR 5798, F-33400 Talence, France*

Driven nanomechanical resonators based on low-dimensional materials are routinely and efficiently detected with electrical mixing measurements. However, the measured signal is a non-trivial combination of the mechanical eigenmode displacement and an electrical contribution, which makes the extraction of the driven mechanical response challenging. Here, we report a simple yet reliable method to extract solely the driven mechanical vibrations by eliminating the contribution of pure electrical origin. This enables us to measure the spectral mechanical response as well as the driven quadratures of motion. We further show how to calibrate the measured signal into units of displacement. Additionally, we utilize the pure electrical contribution to directly determine the effective mass of the measured mechanical mode. Our method marks a key step forward in the study of nanoelectromechanical resonators based on low-dimensional materials in both the linear and the nonlinear regime.

I INTRODUCTION

Nanomechanical resonators [1] are exquisite sensors of mass adsorption [2–4] and external forces [5–8]. These sensing capabilities enable advances in different research fields, such as mass spectrometry [9], surface science [10–12], heat transport [13, 14], in-situ nanofabrication [15], magnetic resonance imaging [16–18], scanning probe microscopy [19–21], nanomagnetism [22–25], and probing viscosity in liquids [26]. Many of these studies are carried out with mechanical resonators based on low-dimensional materials, such as carbon nanotubes [27, 28], because of their tiny mass. However, the detection of motion becomes increasingly difficult as resonators get smaller.

The electrical detection of resonators based on low-dimensional materials is usually realized with a mixing-based method [28, 29], where the vibrations are driven near resonance frequency and detected at a low frequency within the RC bandwidth of the circuit. This down-conversion of the frequency is crucial, since the resonance frequency of the vibrations is usually much larger than the bandwidth imposed by the resistance of the sample and the capacitance of the electrical cables that connect the device to the measurement instruments. Another reason for this frequency down-conversion is to filter out the parasitic background signal of the drive that overwhelms the measured signal of the vibrations; the direct capacitive signal transduction without this mixing rarely works for nanoresonators in contrast to micro- and macro-scale resonators.

The electrical mixing detection has been applied to resonators based on carbon nanotubes [6, 10, 12, 28, 30–46], graphene [35, 47–57], transition metal dichalcogenides (TMDs) [58–63], and semiconducting nanowires [64–71]. Different variants of the mixing method were developed

by applying either two signals [28] on the device or one signal that is amplitude [48] or frequency [33] modulated. The transduction from displacement into current can be based on capacitive [28] or piezo-resistive measurements [72]. Methods were also implemented to measure thermal vibrations [39] and ring-downs [43, 73] at temperatures down to below 0.1 K. The fundamental detection limit was theoretically investigated in Ref. [74]. Despite this large amount of work, the measurement of the spectral response of nanomechanical vibrations to a driving force – the most common method to study mechanical resonators [1] – remains to be demonstrated with the mixing detection.

Here, we report on a simple, yet reliable, method to measure the spectral mechanical response to a driving force using the mixing method with two signals applied to the device. By properly tuning the phase of the measured signal, we are able to separate the signal of the mechanical vibrations from the signal of pure electrical origin inherent to the mixing method. Moreover, we use the pure electrical contribution as a resource to measure the mass of the mechanical eigenmode. The mass is a key parameter of mechanical resonators, but its determination is challenging, especially for resonators based on low-dimensional materials.

II DEVICE AND EXPERIMENTAL APPROACH

We produce nanotube mechanical resonators by growing nanotubes using chemical vapor deposition on prepatterned electrodes. The nanotube is suspended $\simeq 150$ nm above a gate electrode and connected between two metal electrodes [6] (Fig. 1a). We clean the nanotube surface from contamination molecules by applying a large cur-

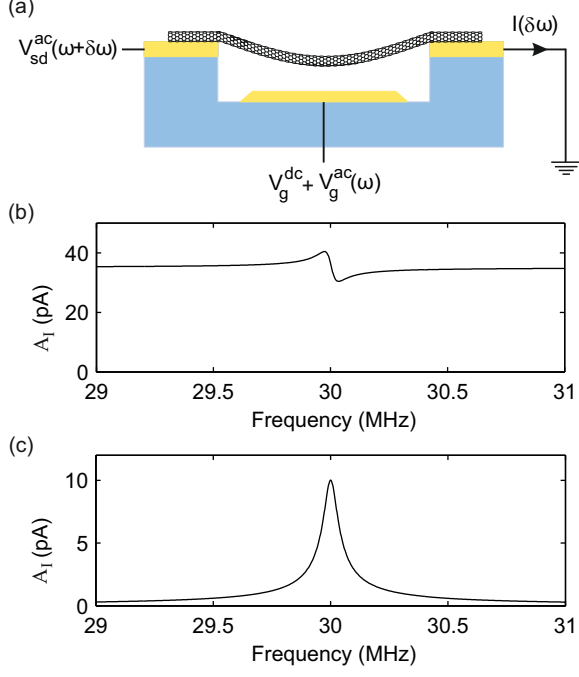


FIG. 1: (a) Schematics of measured device. The nanotube is suspended over a gate electrode and electrically connected to two metal electrodes. Two oscillating voltage signals are applied to the device. The current I is measured with a RLC resonator and a low-temperature amplifier [6]. (b) Calculated response of an underdamped harmonic oscillator electromechanically driven by a capacitive force $F(\omega) \propto V_g^{ac}(\omega)$ expected from the mixing method in the limit where the mechanical displacement is much smaller than $C_g V_g^{ac}/C_g' V_g^{dc}$. (c) Same as panel b but in the opposite limit.

rent through the device under vacuum at low temperature [75].

We detect the vibrations of the nanotube resonator by capacitively driving it with an oscillating voltage $V_g^{ac} \cos \omega t$ on the gate electrode, applying the voltage $V_s^{ac} \cos((\omega + \delta\omega)t + \varphi_e)$ on the source electrode, and measuring the current at frequency $\delta\omega$ from the drain electrode with a lock-in amplifier [6] (Fig. 1a) where φ_e is the phase difference between the two oscillating voltages. We set $\delta\omega$ within the bandwidth of the circuit and we sweep ω through the mechanical frequency ω_m ($\delta\omega \ll \omega_m$). All the measurements are carried out with the device in the single-electron tunneling regime [76–80] at the temperature $T = 6$ K.

To detect the vibrations, the nanotube has to behave as a transistor such that the conductance G depends on the charge Q in the nanotube. The application of $V_g^{ac} \cos \omega t$ modulates the charge through two terms $\delta Q = C_g \delta V_g + \delta C_g V_g$. The first term has a pure electrical origin, while the second term is proportional to the driven vibration displacement δz via $\delta C_g = C_g' \delta z$, where C_g' is the spatial derivative of the capacitance. The application of $V_s^{ac} \cos((\omega + \delta\omega)t + \varphi_e)$ enables one to mix

down the modulation of G into a current oscillation at the frequency $\delta\omega$ within the circuit bandwidth via Ohm's law $I = GV_s$. The mixing intertwines the two terms of the charge modulation. As a result, the displacement of the vibrations driven at frequency ω and the current at frequency $\delta\omega$ given by

$$z = A_z \cos(\omega t + \phi_z) = X_z \cos \omega t + Y_z \sin \omega t, \quad (1)$$

$$I = A_I \cos(\delta\omega t + \phi_I) = X_I \cos \delta\omega t + Y_I \sin \delta\omega t. \quad (2)$$

are related in a cumbersome way, since the quadratures X_I and Y_I of the current depend on the quadratures X_z and Y_z of the displacement as

$$X_I = \alpha [(X_z + C_g V_g^{ac}/C_g' V_g^{dc}) \cos \varphi_e - Y_z \sin \varphi_e], \quad (3)$$

$$Y_I = \alpha [-(X_z + C_g V_g^{ac}/C_g' V_g^{dc}) \sin \varphi_e + Y_z \cos \varphi_e], \quad (4)$$

with $\alpha = (\partial G/\partial V_g) V_s^{ac} V_g^{dc} C_g'/2C_g$, $(\partial G/\partial V_g)$ the transconductance, and V_g^{dc} the static voltage applied to the gate (Appendix A). We note that the work function difference between the nanotube and the gate electrode has to be subtracted from V_g^{dc} .

The downside of the mixing method is that the measured current is not directly proportional to the driven vibration displacement. The amplitude of the current is given by $A_I = \alpha \sqrt{(X_z + C_g V_g^{ac}/C_g' V_g^{dc})^2 + Y_z^2}$. In the limit where the displacement z is much smaller than $C_g V_g^{ac}/C_g' V_g^{dc}$, the response of A_I consists of a signal proportional to X_z together with a large, frequency-independent background that has a pure electrical origin, see Fig. 1b. In the opposite limit, the responses of A_I and A_z become proportional to each other (Fig. 1c).

It is possible to separate the current signal of pure electrical origin by setting $X_I \propto X_z + C_g V_g^{ac}/C_g' V_g^{dc}$ and $Y_I \propto Y_z$ by properly adjusting the phase ϕ_{LIA} of the lock-in amplifier, which enters Eqs. 3,4 by replacing $\varphi_e \rightarrow \varphi_e - \phi_{LIA}$. However, this is not practical, since the phase of the lock-in amplifier often needs to be readjusted when changing V_g^{ac} and V_g^{dc} . Alternatively, the signal of pure electrical origin can be separated after the measurements by performing a rotation of the angle ϕ_I in the plane (X_I, Y_I) for the data. This is equivalent to the transformation $\varphi_e \rightarrow \varphi_e - \phi_{LIA}$. To illustrate this alternative method, we proceed with the response of the two quadratures X_I and Y_I of the current directly acquired from the lock-in amplifier (Figs. 2a,b). The two responses cannot be described by the usual functional forms of driven linear oscillators, since the phase of the lock-in amplifier was not adjusted beforehand. We then compute the background offset of Y_I by incrementing the rotation phase ϕ_I by $\delta\phi_I$ from 0 to 2π (Fig. 2c). When this background offset in Y_I is zero, all the current signal of pure electrical origin is in X_I and can be

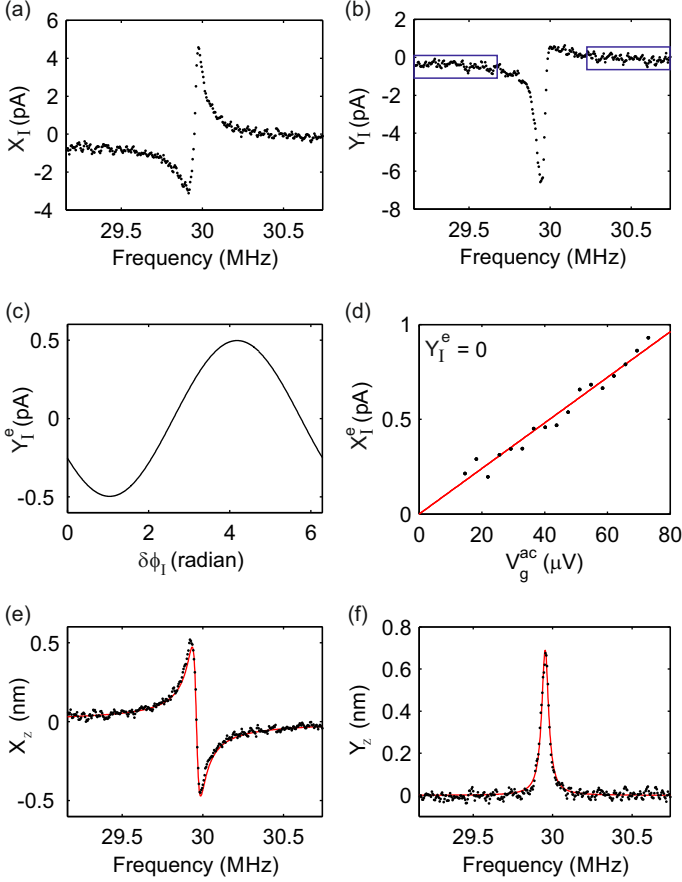


FIG. 2: (a,b) Spectral response of the current quadratures X_I and Y_I to the driven capacitive force. The two blue boxes indicate the Y_I values used to compute the background offset Y_I^e . (c) Estimated background offset Y_I^e from the data in a and b by incrementing the phase ϕ_I in Eq. 1 by $\delta\phi_I$. (d) Background current X_I^e with pure electrical origin with $\delta\phi_I$ set so that $Y_I^e = 0$. The red line is a linear fit of the data. (e,f) Spectral response of the displacement quadratures X_z and Y_z to the driven capacitive force after having subtracted X_I^e from X_I . The data are compared to the quadratures expected for a linear oscillator (red lines).

subtracted from the data. The resulting quadrature responses have now the familiar functional form of linear oscillators (Figs. 2e,f) and the spectral response of the displacement is well described by a Lorentzian (Fig. 3a).

III RESULTS AND DISCUSSION

We use the subtracted background current X_I^e of pure electrical origin to calibrate the displacement of the nanotube resonator in units of meters (Fig. 3a). This background current is given by $X_I^e = (\partial G / \partial V_g) V_s^{\text{ac}} V_g^{\text{ac}} / 2$; we verify that it depends linearly on V_g^{ac} (Fig. 2d). The two

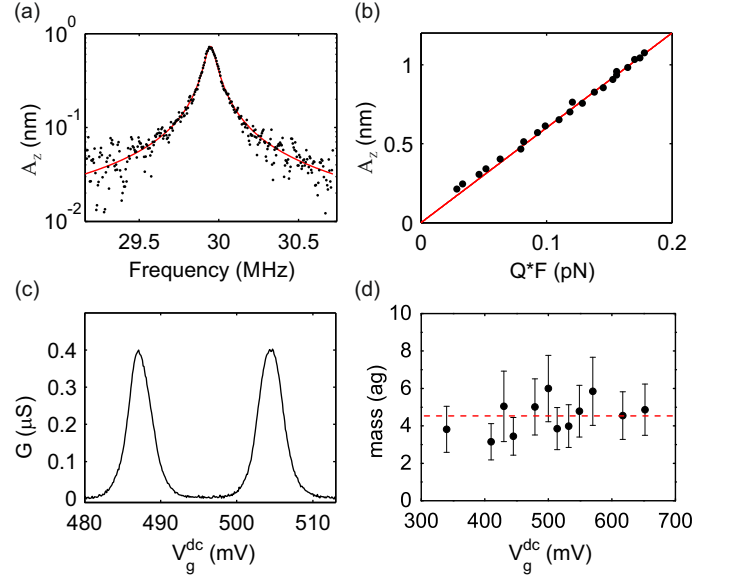


FIG. 3: (a) Spectral response of the displacement amplitude A_z to the driven capacitive force after having subtracted X_I^e from X_I . The data are compared to a Lorentzian peak (red line). (b) Force response of the displacement amplitude A_z at the mechanical resonance frequency. The red line is a linear fit of the data. The force is multiplied by the quality factor, since the latter varies when increasing the driving force [35]. (c) Electrical conductance of the nanotube device as a function of gate voltage. (d) Mass of the eigenmode measured at different gate voltage values. The red dashed line indicates the average mass of 4.5 ag.

quadratures then read:

$$X_z = \frac{C_g V_g^{\text{ac}}}{C'_g V_g^{\text{dc}}} \frac{X_I - X_I^e}{X_I^e}, \quad Y_z = \frac{C_g V_g^{\text{ac}}}{C'_g V_g^{\text{dc}}} \frac{Y_I}{X_I^e}. \quad (5)$$

The calibration of the displacement is subject to the uncertainty in the estimation of C_g/C'_g (see below).

The current X_I^e of pure electrical origin also enables quantifying the mass of the mechanical mode in a way that is simple and reliable. In Fig. 3b, we compute the force response of the displacement amplitude at resonance frequency ω_m in the linear regime using

$$A_z = \frac{C_g V_g^{\text{ac}}}{C'_g V_g^{\text{dc}}} \frac{Y_I}{X_I^e}, \quad F = \beta C'_g V_g^{\text{dc}} V_g^{\text{ac}}, \quad (6)$$

where Y_I corresponds to the current amplitude at resonance frequency after having separated the signal of pure electrical origin. The constant β can be different from one for electron transport in the single-electron regime (Eq. 7 and Appendix A). The mass m is determined from the slope of the force-displacement response using $A_z = (Q/m\omega_m^2)F$ with Q the quality factor. The slope depends on the current terms Y_I and X_I^e measured from the lock-in amplifier, but is independent of V_g^{ac} , V_s^{ac} , and $\partial G / \partial V_g$ that enter the prefactor α in the current-displacement conversion in Eqs. 3,4 and whose values

could be somewhat altered by the amplification chain and the losses along the coaxial cables. We determine $m = 4.5 \pm 1.5$ ag from the mass measured at different V_g^{dc} values (Fig. 3d). This value is consistent with the length of the suspended nanotube measured by scanning electron microscopy and assuming a 1.5 nm radius single-wall nanotube.

The uncertainty in the mass measurement comes from the uncertainty in the estimation of the nanotube-gate separation d and the mass fluctuations in Fig. 3d. The separation $d = 150 \pm 20$ nm measured by atomic force microscopy enters in the estimation of $C'_g = C_g/d \ln(2d/r)$ in Eqs. 5,6 when considering the capacitance between a tube with radius r separated from a plate by the distance d . We estimate $C_g = e/\Delta V_g = 9.7$ aF from the separation ΔV_g in gate voltage between two conductance peaks associated with single-electron tunneling (Fig. 3c). This capacitance is consistent with $C_g = 12.9$ aF obtained from the device geometry measured by scanning electron microscopy and atomic force microscopy. The fluctuations of m in Fig. 3d are partly due to the error in the estimation of the average charge occupation f , which varies between 0 and 1 when sweeping V_g^{dc} through the conductance peaks (Fig. 3c), since f enters in the prefactor β of the driven force in Eq. 6 as

$$\beta = 1 - \frac{C_g}{C_\Sigma} + f(1 - f) \frac{C_g}{C_\Sigma} \frac{e^2/C_\Sigma}{k_B T}, \quad (7)$$

in the incoherent single-electron tunneling regime. Here, C_Σ is the total capacitance of the single-electron transistor and varies gradually from 19.9 aF to 26.5 aF when sweeping V_g^{dc} over multiple conductance peaks. The fluctuations of m are also attributed to the slow increase of the contamination on the nanotube surface at 6 K; the three largest m values in Fig. 3d are obtained from force-displacement measurements carried out one month after the first measurements.

IV CONCLUSION

In summary, we show how to measure the spectral mechanical response using electrical mixing measurements. Our method enables us to calibrate the displacement in meters. Another asset of this method is the determination of the mass of the measured mechanical eigenmode, which is a key parameter of the mechanical resonators when used in sensor applications. This work opens the possibility to quantitatively study nanoelectromechanical resonators in the nonlinear regime, where different mesoscopic phenomena can be explored [1]. In previous studies, the shape of the nonlinear response measured with the mixing method was often complicated and it was not possible to unambiguously separate the contribution of the nonlinear mechanical response from the contribution with a pure electrical origin. By contrast, it is expected

that our method is able to extract the nonlinear mechanical response in a straightforward way.

V ACKNOWLEDGEMENTS

We acknowledge ERC Advanced Grant No. 692876 and MICINN Grant No. RTI2018-097953-B-I00. Work performed at the Center for Nanoscale Materials, a U.S. Department of Energy Office of Science User Facility, was supported by the U.S. DOE, Office of Basic Energy Sciences, under Contract No. DE-AC02-06CH11357. We also acknowledge AGAUR (Grant No. 2017SGR1664), the Fondo Europeo de Desarrollo, the Spanish Ministry of Economy and Competitiveness through Quantum CCAA and CEX2019-000910-S [MCIN/ AEI/10.13039/501100011033], Fundacio Cellex, Fundacio Mir-Puig, Generalitat de Catalunya through CERCA, the French Agence Nationale de la Recherche (Grant No. SINPHOCOM ANR-19-CE47-0012), Marie Skłodowska-Curie (Grant No. 101023289).

APPENDIX A: TWO-SOURCE MIXING METHOD

We consider a double-clamped mechanical resonator that is capacitively coupled to an immobile gate electrode. The two-source mixing method requires that the conductance through the resonator varies when sweeping the gate voltage. In what follows, we consider the regime of single-electron tunneling, but the same final result for the mixing current is obtained for any other regime. The vibrations are driven by applying an oscillating voltage $V_g^{\text{ac}} \cos \omega t$ on the gate electrode. When applying the voltage $V_s^{\text{ac}} \cos((\omega + \delta\omega)t + \varphi_e)$ on the source electrode, the mixing current at frequency $\delta\omega$ arises in the Taylor expansion of the current in z and V_g [28]. The dependence of the current on these two quantities can be traced back to the tunnelling rate dependence on the electrostatic energy difference between the two relevant charge states of the dot. For vanishing bias voltage the electrostatic energy reads $E_E(Q) = (Q + C_g(z)V_g)^2/2C_\Sigma(z)$ with C_g and C_Σ the gate and total capacitances and Q the charge on the dot. This gives for the relevant energy difference $\Delta E = E_E(Q - e) - E_E(Q) = e(e/2 - Q - C_g(z)V_g)/C_\Sigma(z)$. The current is then a function of $\Delta E(z, V_g)$. Expanding the current expression for $eV_s \ll k_B T$, small displacement z [given by Eq. (1)], and V_g^{ac} one obtains:

$$I = \frac{\partial G}{\partial V_g} V_s^{\text{ac}} \cos((\omega + \delta\omega)t + \varphi_e) \times [V_g^{\text{ac}} \cos \omega t + V_g^{\text{dc}} C'_g/C_g [X_z \cos(\omega t) + Y_z \sin(\omega t)]]. \quad (8)$$

Here $\partial G/\partial V_g$ is the transconductance of the nanotube device, V_g^{dc} the static voltage applied to the gate and we

assumed $Q \approx -C_g V_g \gg e$. Expanding the argument of the first cosine and averaging over a period $2\pi/\omega$ gives the mixing current $I^{\delta\omega}$ at frequency $\delta\omega$:

$$I^{\delta\omega} = \frac{1}{2} \frac{\partial G}{\partial V_g} V_s^{\text{ac}} \left[\cos(\delta\omega t + \varphi_e) \left(V_g^{\text{ac}} + \frac{V_g^{\text{dc}} C'_g}{C_g} X_z \right) - \sin(\delta\omega t + \varphi_e) \frac{V_g^{\text{ac}} C'_g}{C_g} Y_z \right]. \quad (9)$$

This leads to the mixing current quadratures X_I and Y_I in Eqs. 3,4. The expression of the mixing current in Eq. 9 is the same for other types of conductors, such as the electronic Farby-Pérot interferometer or the the field-effect transistor [28]. In the next appendix, we show that the capacitive force in the single-electron tunneling regime is different from that in other regimes.

APPENDIX B: DRIVING FORCE IN THE SINGLE-ELECTRON TUNNELING REGIME

We discuss here the oscillating force acting on a mechanical resonator hosting a dot that behaves as a single-electron transistor in the limit typically realized in experiments with a slow oscillator $\Gamma \gg \omega_m$, where Γ is the typical incoherent tunneling rate ($k_B T \gg \hbar \Gamma$). When the gate voltage is modulated, the charge on the dot changes, leading to an additional oscillating force acting on the oscillator. This is the reason why the constant β in Eq. 6 for the capacitive force can deviate from one. The total capacitive force between the resonator and the the gate electrode can be written as

$$F = -\frac{\partial}{\partial z} \frac{Q_g^2}{2C_g(z)} = \frac{Q_g^2 C'_g}{2C_g^2} \quad (10)$$

where Q_g is the charge on the gate electrode (we assume that the capacitances to the source or drain are not modified by the displacement of the resonator). In the sequential tunnelling regime the charge on the dot is always an integer multiple of the elementary charge $Q = -e(n_0 + n)$, with n_0 and n integers, and only n varies between 0 and 1. From electrostatics the gate charge is then:

$$Q_g = C_g V_g - \frac{C_g}{C_\Sigma} (V_s C_s + C_d V_d + C_g V_g + Q). \quad (11)$$

where we introduced the source and drain voltages (V_s, V_d) and capacitances (C_s, C_d) with $C_\Sigma = C_g + C_s + C_d$. Since the number of electrons fluctuates of one unit during transport, there are actually two forces acting on the dot, one for each value of Q . Using the separation of time scales we can assume that the oscillator cannot respond to the fast electron fluctuations, and thus it feels an average force given by the average value of Q . When $\delta V_g(t) = V_g^{\text{ac}} \cos(\omega t)$ is applied to the gate electrode, we

can write that the resulting variation of the charge on the gate electrode reads:

$$\delta Q_g = C_g \delta V_g \left[1 - \frac{C_g}{C_\Sigma} \right] + \frac{C_g}{C_\Sigma} \delta \langle Q \rangle. \quad (12)$$

We can neglect the higher orders in the z -dependence of the capacitance when computing the force in Eq. 10, since this gives rise only to a renormalization of the resonance frequency. The variation of Q is controlled by the master equation for the charge. Assuming that only two charge states are possible, one has $\langle Q \rangle = -n_0 e - e f$ with f the Fermi function $f = (e^{\varepsilon/k_B T} + 1)^{-1}$ where the ε dependence on the gate voltage is $\delta \varepsilon = -e C_g \delta V_g / C_\Sigma$. We obtain then

$$\delta \langle Q \rangle = -\frac{e^2}{k_B T} \frac{C_g}{C_\Sigma} \delta V_g f(1-f). \quad (13)$$

Note that the factor $(e^2/C_\Sigma)/k_B T \gg 1$ in the Coulomb blockade regime. This term $\delta \langle Q \rangle$ is largest for gate voltages at which the peak conductance is highest and where $f = 1/2$. Inserting Eq. 13 into Eq. 12 and Eq. 10 one obtains Eq. 7 of the main text.

For completeness, it can be useful to recall the derivation of the coupling constant between the mechanical and electronic degrees of freedom. This is the variation of the force acting on the oscillator when an electron on the dot is added or removed.

$$F_0 = F_g(Q) - F_g(Q - e) = \frac{C'_g e^2}{C_g C_\Sigma} (Q_g/e - 1). \quad (14)$$

For $|Q_g| \gg e$ and $V_s \approx V_d \approx 0$ one finds

$$F_0 = \frac{C'_g V_g e}{C_\Sigma}. \quad (15)$$

-
- [1] Bachtold, A., Moser, J. & Dykman, M. I. Mesoscopic physics of nanomechanical systems. *arXiv preprint arXiv:2202.01819* (2022).
 - [2] Yang, Y. T., Callegari, C., Feng, X. L., Ekinci, K. L. & Roukes, M. L. Zeptogram-Scale Nanomechanical Mass Sensing. *Nano Lett* **6**, 583–586 (2006).
 - [3] Chaste, J. *et al.* A Nanomechanical Mass Sensor with Yoctogram Resolution. *Nat Nano* **7**, 301–304 (2012).
 - [4] Malvar, O. *et al.* Mass and stiffness spectrometry of nanoparticles and whole intact bacteria by multimode nanomechanical resonators. *Nat. Commun.* **7**, 1–8 (2016).
 - [5] Gavartin, E., Verlot, P. & Kippenberg, T. J. A hybrid on-chip optomechanical transducer for ultrasensitive force measurements. *Nature nanotechnology* **7**, 509–514 (2012).
 - [6] de Bonis, S. L. *et al.* Ultrasensitive displacement noise measurement of carbon nanotube mechanical resonators. *Nano Lett.* **18**, 5324–5328 (2018).

- [7] Heritier, M. *et al.* Nanoladder cantilevers made from diamond and silicon. *Nano Lett.* **18**, 1814–1818 (2018).
- [8] Sahafi, P. *et al.* Ultralow dissipation patterned silicon nanowire arrays for scanning probe microscopy. *Nano Lett.* **20**, 218–223 (2020).
- [9] Hanay, M. S. *et al.* Single-protein nanomechanical mass spectrometry in real time. *Nature Nanotechnology* **7**, 602–608 (2012).
- [10] Wang, Z. *et al.* Phase Transitions of Adsorbed Atoms on the Surface of a Carbon Nanotube. *Science* **327**, 552–555 (2010).
- [11] Yang, Y. T., Callegari, C., Feng, X. L. & Roukes, M. L. Surface Adsorbates Fluctuations and Noise in Nanoelectromechanical Systems. *Nano Lett.* **11**, 1753 (2011).
- [12] Noury, A. *et al.* Layering Transition in Superfluid Helium Adsorbed on a Carbon Nanotube Mechanical Resonator. *Phys. Rev. Lett.* **122**, 165301 (2019).
- [13] Morell, N. *et al.* Optomechanical measurement of thermal transport in two-dimensional MoSe₂ lattices. *Nano Lett.* **19**, 3143–3150 (2019).
- [14] Dolleman, R. J., Verbiest, G. J., Blanter, Y. M., van der Zant, H. S. J. & Steeneken, P. G. Nonequilibrium thermodynamics of acoustic phonons in suspended graphene. *Phys. Rev. Research* **2**, 012058 (2020).
- [15] Gruber, G. *et al.* Mass Sensing for the Advanced Fabrication of Nanomechanical Resonators. *Nano Lett.* **19**, 6987–6992 (2019).
- [16] Degen, C. L., Poggio, M., Mamin, H. J., Rettner, C. T. & Rugar, D. Nanoscale magnetic resonance imaging. *Proc Natl Acad Sci USA* **106**, 1313 (2009).
- [17] Rose, W. *et al.* High-resolution nanoscale solid-state nuclear magnetic resonance spectroscopy. *PRX* **8**, 011030 (2018).
- [18] Grob, U. *et al.* Magnetic resonance force microscopy with a one-dimensional resolution of 0.9 nanometers. *Nano Lett.* **19**, 7935–7940 (2019).
- [19] Li, M., Tang, H. X. & Roukes, M. L. Ultra-Sensitive NEMS-Based Cantilevers for Sensing, Scanned Probe and Very High-Frequency Applications. *Nat. Nanotechnol.* **2**, 114–120 (2007).
- [20] de Lépinay, L. M. *et al.* A universal and ultrasensitive vectorial nanomechanical sensor for imaging 2d force fields. *Nature Nanotechnology* **12**, 156 (2016).
- [21] Rossi, N. *et al.* Vectorial scanning force microscopy using a nanowire sensor. *Nature Nanotechnology* **12**, 150 (2016).
- [22] Losby, J. E. *et al.* Torque-mixing magnetic resonance spectroscopy. *Science* **350**, 798 (2015).
- [23] Rossi, N., Gross, B., Dirnberger, F., Bougeard, D. & Poggio, M. Magnetic force sensing using a self-assembled nanowire. *Nano Lett.* **19**, 930–936 (2019).
- [24] Šiškins, M. *et al.* Magnetic and electronic phase transitions probed by nanomechanical resonators. *Nature Communications* **11**, 2698 (2020).
- [25] Jiang, S., Xie, H., Shan, J. & Mak, K. F. Exchange magnetostriction in two-dimensional antiferromagnets. *Nature Materials* **19**, 1295–1299 (2020).
- [26] Gil-Santos, E. *et al.* High-frequency nano-optomechanical disk resonators in liquids. *Nat. Nanotechnol.* **10**, 810–816 (2015).
- [27] Reulet, B. *et al.* Acoustoelectric effects in carbon nanotubes. *Phys. Rev. Lett.* **85**, 2829–2832 (2000).
- [28] Sazonova, V. *et al.* A tunable carbon nanotube electromechanical oscillator. *Nature* **431**, 284–287 (2004).
- [29] Knobel, R. G. & Cleland, A. N. Nanometre-scale displacement sensing using a single electron transistor. *Nature* **424**, 291 (2003).
- [30] Witkamp, B., Poot, M. & van der Zant, H. S. J. Bending-mode vibration of a suspended nanotube resonator. *Nano letters* **6**, 2904–2908 (2006).
- [31] Chiu, H.-Y., Hung, P., Postma, H. W. C. & Bockrath, M. Atomic-scale mass sensing using carbon nanotube resonators. *Nano letters* **8**, 4342–4346 (2008).
- [32] Lassagne, B., Tarakanov, Y., Kinaret, D., J. and Garcia-Sanchez & Bachtold, A. Coupling mechanics to charge transport in carbon nanotube mechanical resonators. *Science* **325**, 1107–1110 (2009).
- [33] Gouttenoire, V. *et al.* Digital and FM Demodulation of a Doubly Clamped Single-Walled Carbon-Nanotube Oscillator: Towards a Nanotube Cell Phone. *Small* **6**, 1060–1065 (2010).
- [34] Wu, C. C. & Zhong, Z. Capacitive spring softening in single-walled carbon nanotube nanoelectromechanical resonators. *Nano Letters* **11**, 1448–1451 (2011).
- [35] Eichler, A. *et al.* Nonlinear damping in mechanical resonators made from carbon nanotubes and graphene. *Nature nanotechnology* **6**, 339–342 (2011).
- [36] Eichler, A., Chaste, J., Moser, J. & Bachtold, A. Parametric amplification and self-oscillation in a nanotube mechanical resonator. *Nano letters* **11**, 2699–2703 (2011).
- [37] Laird, E. A., Pei, F., Tang, W., Steele, G. A. & Kouwenhoven, L. P. A high quality factor carbon nanotube mechanical resonator at 39 ghz. *Nano letters* **12**, 193–197 (2012).
- [38] Eichler, A., Moser, M. I., J. and Dykman & Bachtold, A. Symmetry breaking in a mechanical resonator made from a carbon nanotube. *Nature communications* **4**, 1–7 (2013).
- [39] Moser, J. *et al.* Ultrasensitive Force Detection with a Nanotube Mechanical Resonator. *Nat Nanotech* **8**, 493 (2013).
- [40] Lee, S.-W., Truax, S., Yu, L., Roman, C. & Hierold, C. Carbon nanotube resonators with capacitive and piezoresistive current modulation readout. *Applied Physics Letters* **103**, 033117 (2013).
- [41] Moser, J., Eichler, A., Güttinger, J., Dykman, M. I. & Bachtold, A. Nanotube mechanical resonators with quality factors of up to 5 million. *Nature nanotechnology* **9**, 1007–1011 (2014).
- [42] Benyamini, A., Hamo, A., Kusminskiy, S. V., von Oppen, F. & Ilani, S. Real-space tailoring of the electron–phonon coupling in ultraclean nanotube mechanical resonators. *Nature Physics* **10**, 151–156 (2014).
- [43] Schneider, B. H., Singh, V., Venstra, W. J., Meerwaldt, H. B. & Steele, G. A. Observation of Decoherence in a Carbon Nanotube Mechanical Resonator. *Nat Commun* **5**, 5819 (2014).
- [44] Kumar, L., Jenni, L. V., Haluska, M., Roman, C. & Hierold, C. Mechanical stress relaxation in adhesively clamped carbon nanotube resonators. *AIP Advances* **8**, 025118 (2018).
- [45] Khivrich, I., Clerk, A. A. & Ilani, S. Nanomechanical pump-probe measurements of insulating electronic states in a carbon nanotube. *Nature Nanotechnology* **14**, 161–167 (2019).
- [46] Rechnitz, S., Tabachnik, T., Shlafman, M., Shlafman,

- S. & Yaish, Y. Mode coupling, bi-stability, and spectral broadening in buckled nanotube resonators. *arXiv preprint arXiv:2110.01572* (2021).
- [47] Chen, C. *et al.* Performance of monolayer graphene nanomechanical resonators with electrical readout. *Nature nanotechnology* **4**, 861–867 (2009).
- [48] Zande, A. M. v. d. *et al.* Large-scale arrays of single-layer graphene resonators. *Nano letters* **10**, 4869–4873 (2010).
- [49] Singh, V. *et al.* Probing thermal expansion of graphene and modal dispersion at low-temperature using graphene nanoelectromechanical systems resonators. *Nanotechnology* **21**, 165204 (2010).
- [50] Singh, V. *et al.* Coupling between quantum hall state and electromechanics in suspended graphene resonator. *Applied Physics Letters* **100**, 233103 (2012).
- [51] Miao, T., Yeom, S., Wang, B., P. and Standley & Bockrath, M. Graphene nanoelectromechanical systems as stochastic-frequency oscillators. *Nano letters* **14**, 2982–2987 (2014).
- [52] Parmar, M. M., Gangavarapu, P. R. Y. & Naik, A. K. Dynamic range tuning of graphene nanoresonators. *Applied Physics Letters* **107**, 113108 (2015).
- [53] Verbiest, G. J. *et al.* Detecting ultrasound vibrations with graphene resonators. *Nano letters* **18**, 5132–5137 (2018).
- [54] Luo, G. *et al.* Strong indirect coupling between graphene-based mechanical resonators via a phonon cavity. *Nature Communications* **9**, 383 (2018).
- [55] Jung, M. *et al.* Ghz nanomechanical resonator in an ultraclean suspended graphene p–n junction. *Nanoscale* **11**, 4355–4361 (2019).
- [56] Zhang, Z. Z. *et al.* Coherent phonon dynamics in spatially separated graphene mechanical resonators. *Proceedings of the National Academy of Sciences* **117**, 5582–5587 (2020).
- [57] Verbiest, G. *et al.* Tunable coupling of two mechanical resonators by a graphene membrane. *2D Materials* **8**, 035039 (2021).
- [58] Samanta, C., Yavasvi Gangavarapu, P. R. & Naik, A. K. Nonlinear mode coupling and internal resonances in mos2 nanoelectromechanical system. *Applied physics letters* **107**, 173110 (2015).
- [59] Yang, R., Wang, Z. & Feng, P. X. L. All-electrical readout of atomically-thin mos2 nanoelectromechanical resonators in the vhf band. In *2016 IEEE 29th International Conference on Micro Electro Mechanical Systems (MEMS)*, 59–62 (IEEE, 2016).
- [60] Yang, R., Chen, C., Lee, J., Czaplewski, D. A. & Feng, P. X. L. Local-gate electrical actuation, detection, and tuning of atomic-layer mos2 nanoelectromechanical resonators. In *2017 IEEE 30th International Conference on Micro Electro Mechanical Systems (MEMS)*, 163–166 (IEEE, 2017).
- [61] Samanta, C., Arora, N. & Naik, A. K. Tuning of geometric nonlinearity in ultrathin nanoelectromechanical systems. *Applied Physics Letters* **113**, 113101 (2018).
- [62] Manzeli, S., Dumcenco, D., Miglato Marega, G. & Kis, A. Self-sensing, tunable monolayer mos2 nanoelectromechanical resonators. *Nature communications* **10**, 1–7 (2019).
- [63] Sengupta, S., Solanki, H. S., Singh, V., Dhara, S. & Deshmukh, M. M. Electromechanical resonators as probes of the charge density wave transition at the nanoscale in nbse 2. *Physical Review B* **82**, 155432 (2010).
- [64] Solanki, H. S. *et al.* Tuning mechanical modes and influence of charge screening in nanowire resonators. *Physical Review B* **81**, 115459 (2010).
- [65] Mile, E. *et al.* In-plane nanoelectromechanical resonators based on silicon nanowire piezoresistive detection. *Nanotechnology* **21**, 165504 (2010).
- [66] Bargatin, I., Myers, E. B., Arlett, J., Gudlewski, B. & Roukes, M. L. Sensitive detection of nanomechanical motion using piezoresistive signal downmixing. *Applied Physics Letters* **86**, 133109 (2005).
- [67] Bargatin, I., Kozinsky, I. & Roukes, M. L. Efficient electrothermal actuation of multiple modes of high-frequency nanoelectromechanical resonators. *Applied Physics Letters* **90**, 093116 (2007).
- [68] He, R., Feng, X. L., Roukes, M. L. & Yang, P. Self-transducing silicon nanowire electromechanical systems at room temperature. *Nano letters* **8**, 1756–1761 (2008).
- [69] Fung, W. Y., Dattoli, E. N. & Lu, W. Radio frequency nanowire resonators and in situ frequency tuning. *Applied Physics Letters* **94**, 203104 (2009).
- [70] Koumela, A. *et al.* High frequency top-down junction-less silicon nanowire resonators. *Nanotechnology* **24**, 435203 (2013).
- [71] Sansa, M., Fernandez-Regulez, M., San Paulo, Á. & Perez-Murano, F. Electrical transduction in nanomechanical resonators based on doubly clamped bottom-up silicon nanowires. *Applied Physics Letters* **101**, 243115 (2012).
- [72] Sansa, M., Fernandez-Regulez, M., Llobet, J., San Paulo, Á. & Perez-Murano, F. High-sensitivity linear piezoresistive transduction for nanomechanical beam resonators. *Nature Communications* **5**, 4313 (2014).
- [73] Urgell, C. *et al.* Cooling and self-oscillation in a nanotube electromechanical resonator. *Nat. Phys.* **16**, 32–37 (2020).
- [74] Wang, Y. & Pistolesi, F. Sensitivity of mixing-current technique to detect nanomechanical motion. *Phys. Rev. B* **95**, 035410 (2017).
- [75] Yang, W. *et al.* Fabry-pérot oscillations in correlated carbon nanotubes. *Phys. Rev. Lett.* **125**, 187701 (2020).
- [76] Armour, A. D., Blencowe, M. P. & Zhang, Y. Classical Dynamics of a Nanomechanical Resonator Coupled to a Single-Electron Transistor. *Phys Rev B* **69**, 125313 (2004).
- [77] Clerk, A. A. & Bennett, S. Quantum Nanoelectromechanics with Electrons, Quasi-Particles and Cooper Pairs: Effective Bath Descriptions and Strong Feedback Effects. *New J Phys* **7**, 238 (2005).
- [78] Pistolesi, F. & Labarthe, S. Current Blockade in Classical Single-Electron Nanomechanical Resonator. *Phys. Rev. B* **76**, 165317 (2007).
- [79] Usmani, O., Blanter, Y. M. & Nazarov, Y. V. Strong Feedback and Current Noise in Nanoelectromechanical Systems. *Phys Rev B* **75**, 195312 (2007).
- [80] Micchi, G., Avriller, R. & Pistolesi, F. Mechanical signatures of the current blockade instability in suspended carbon nanotubes. *Phys Rev Lett* **115**, 206802 (2015).